

## Fault diagnosis for photovoltaic array based on convolutional neural network and electrical time series graph



Xiaoyang Lu<sup>a,b</sup>, Peijie Lin<sup>a,b,\*</sup>, Shuying Cheng<sup>a,b,\*</sup>, Yaohai Lin<sup>c</sup>, Zhicong Chen<sup>a,b</sup>, Lijun Wu<sup>a,b</sup>, Qianying Zheng<sup>a,b</sup>

<sup>a</sup> School of Physics and Information Engineering, and Institute of Micro-Nano Devices and Solar Cells, Fuzhou University, Fuzhou, China

<sup>b</sup> Jiangsu Collaborative Innovation Center of Photovoltaic Science and Engineering, Changzhou, China

<sup>c</sup> College of Computer and Information Sciences, Fujian Agriculture and Forest University, Fuzhou, China

### ARTICLE INFO

**Keywords:**

Photovoltaic array  
Fault diagnosis  
Electrical time series graph  
Deep learning  
Convolutional neural network

### ABSTRACT

Fault diagnosis of photovoltaic array plays an important role in operation and maintenance of PV power plant. The nonlinear characteristics of photovoltaic array and the Maximum Power Point Tracking technology in the inverter prevent conventional protection devices to trip under certain faults which reduces the system's efficiency and increases the risks of fire hazards. In order to better diagnose photovoltaic array faults under Maximum Power Point Tracking conditions, the sequential data of transient in time domain under faults are analyzed and then applied as the input fault features in this work. Firstly, the sequential current and voltage of the photovoltaic array are transformed into a 2-Dimension electrical time series graph to visually represent the characteristics of sequential data. Secondly, a Convolutional Neural Network structure comprising nine convolutional layers, nine max-pooling layers, and a fully connected layer is proposed for the photovoltaic array fault diagnosis. The proposed model for photovoltaic array fault diagnosis integrates two main parts, namely the feature extraction and the classification. Thirdly, this model automatically extracts suitable features representation from raw electrical time series graph, which eliminates the need of using artificially established features of data and then employs for photovoltaic fault diagnosis. Moreover, the proposed Convolutional Neural Network based photovoltaic array fault diagnosis method only takes the array of voltage and current of the photovoltaic array as the input features and the reference panels used for normalization. The proposed approach of photovoltaic array fault diagnosis achieved over 99% average accuracy when applied to the case studies. The comparisons of the experimental results demonstrate that the proposed method is both effective and reliable.

### 1. Introduction

For the last few decades, constant depletion of fossil fuel has promoted the applications of renewable energy [1]. Among these renewable energy, solar energy is one of the most appealing power sources with the advantage of being inexhaustible, cleaning and economical [2]. By the end of 2017, the global photovoltaic (PV) capacity has increased to 402 GW [3]. However, the faults occur in PV array (PVA) drastically impede the efficiency and safety of PV system (PVS) and even cause fire hazards. In order to ensure efficiency and safe operation of PVS, some protective measures should be accompanied with these installations.

Conventionally, the electronic protection devices, such as fuses and circuit breakers, have been applied on PVS to effectively prevent from

accidents [4]. Moreover, a lot of maximum power point tracker (MPPT) techniques are also applied in PVS to maximize the power output of the PVA [5]. These MPPT algorithms can improve output power of PVS by searching maximum power point (MPP) quickly [6] and precisely [7]. Although the MPPT optimizes the power output, it may impede these electronic protection devices to detect faults. When a fault occurs, the output current and voltage of PVA deviate from those of normal condition drastically, leading an unexpected power drop. And then the MPPT keeps searching a new MPP until it is converged, which leads to an electrical transient process in time domain. Finally, when MPPT has converged, The PVS achieves a new steady-state, namely post-fault stage (PSS), the change of PVA current and PVA voltage are not as significant as they are in transient process in time domain [8]. As a result, the quick optimization of MPPT may cause that PVA current and

\* Corresponding authors at: School of Physics and Information Engineering, and Institute of Micro-Nano Devices and Solar Cells, Fuzhou University, 350116 Fuzhou, China.

E-mail addresses: [linpeijie@fzu.edu.cn](mailto:linpeijie@fzu.edu.cn) (P. Lin), [sycheng@fzu.edu.cn](mailto:sycheng@fzu.edu.cn) (S. Cheng).

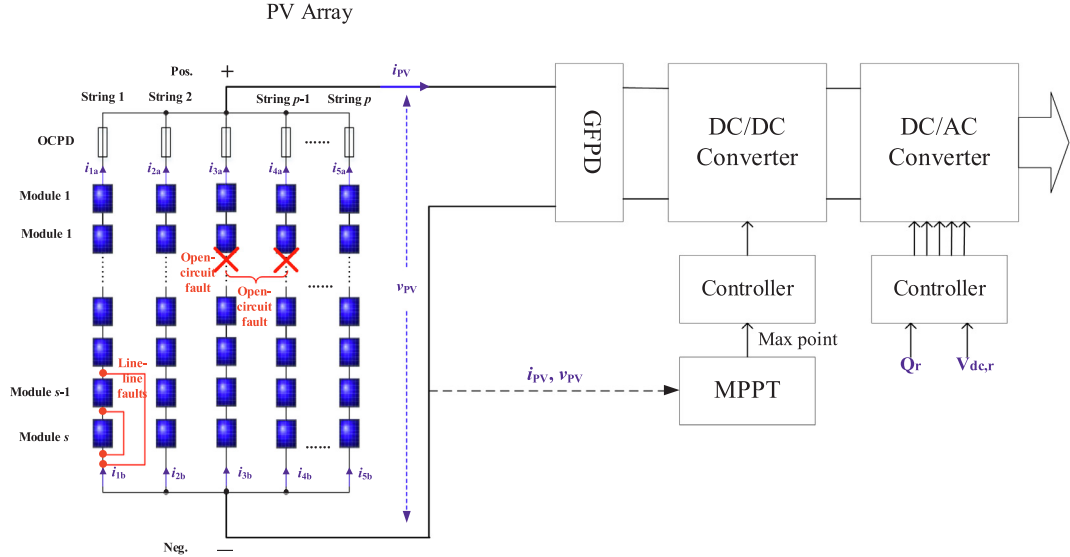
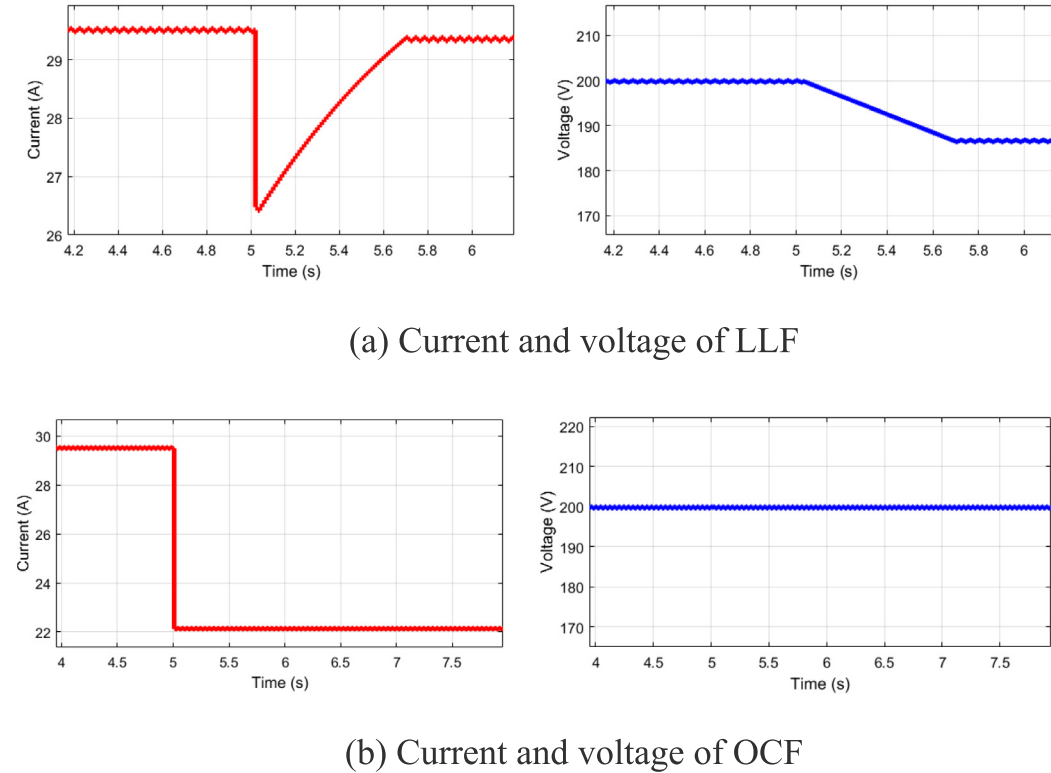


Fig. 1. The typical topology of a PVS.

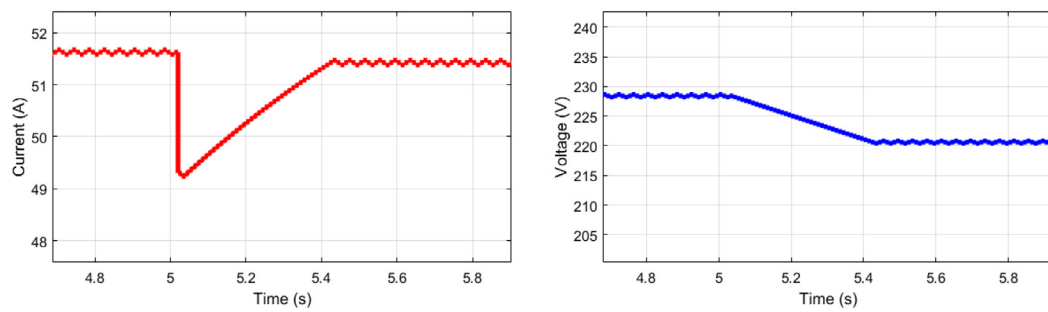
Fig. 2. LLF and OCF sequential PV data curves in  $4 \times 7$  PVS.

PVA voltage fast fall back to the normal range [9], which may impede the protection function of fuses and circuit breakers.

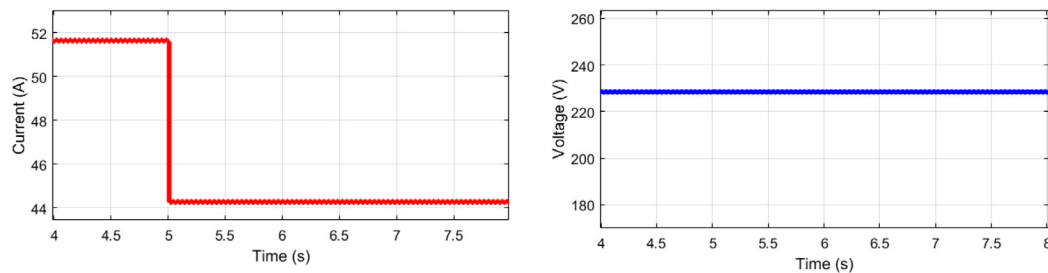
Hence, a few offline inspection methods are introduced to diagnose PVA faults such as I-V characteristics analysis (I-VCA) [10], earth capacitance measurements (ECM) [11], time domain reflectometry (TDR) [12]. Although these off-line methods are not limited to MPPT, which require interrupt the normal operation of PVS. To address this issue, many on-line fault detection and diagnosis (FDD) methods have been presented in the literatures to safeguard PVS from faults when MPPT is in-service. For instance, the power losses analysis methods (PLA) compare the measured DC PV power [13] or the measured AC PV power

[14] with those of the simulated PV power to diagnose PV faults, respectively. Some PLA estimate PV power through satellite image to calculate power loss between measured PV power and estimated PV power [15]. Additionally, the voltage and current measurements (VCM) is proposed to diagnose PVA faults through the comparison between the measured indicators with the specific user-defined thresholds [16]. However, these approaches require rigorous analysis of the system under different states to configure reliable threshold values, which restricts the model performance.

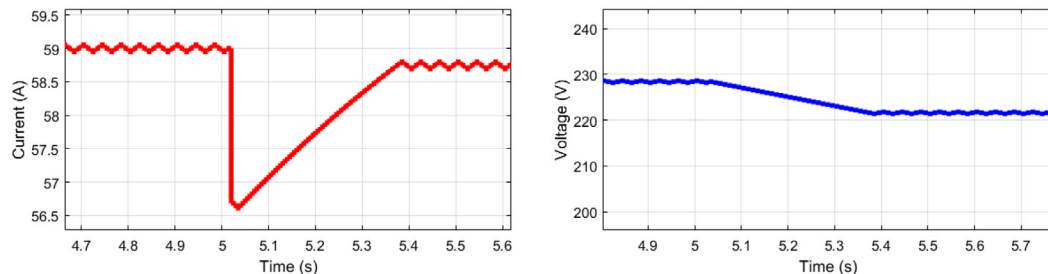
Recently, artificial intelligence techniques (AIT) have been proven their capability for FDD [17]. AIT based approaches can be mainly



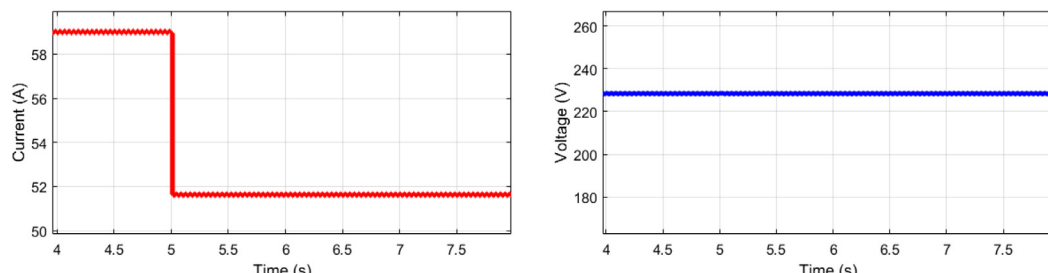
(a) Current and voltage of LLF



(b) Current and voltage of OCF

Fig. 3. LLF and OCF sequential PV data curves in  $7 \times 8$  PVS.

(a) Current and voltage of LLF



(b) Current and voltage of OCF

Fig. 4. LLF and OCF sequential PV data curves in  $8 \times 8$  PVS.

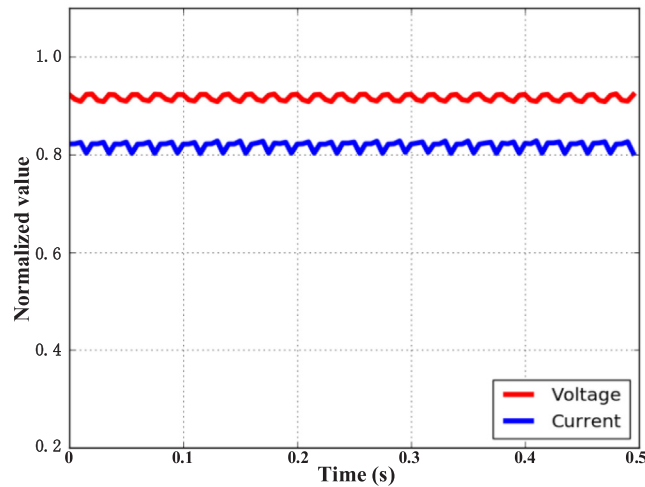


Fig. 5. PVA current and voltage under normal condition.

divided into two categories: steady-state analysis based methods (SSAMs) and transient time-domain analysis based methods (TTDAMs). The SSAMs analyze the PV data of the PV power system operating at PSS and then apply them for FDD. In a certain PVS, different faults result in various PV data in PSS, which leads a sensitivity of SSAMs model to PVA faults. The sensitivity of SSAMs to PVA faults promotes the development of SSAMs in PVA fault diagnosis. There are two kinds of SSAMs, including methods based on a large amount of labeled data and methods based on a few labeled data, and the former are widely used. By applying decision trees (DT) on FDD, PV faults can be diagnosed very quickly without too many steps [18]. Support vector machine (SVM) is a widely used machine learning algorithm and has good noise tolerance and capacity for classification, which can be effective for FDD [19]. As a kind of ensemble learning methods, random forest also shows its powerful ability on FDD, which has high accuracy, strong generalization performance and robustness to noise [20]. The artificial neural network (ANN) is utilized as the identification tool for PV fault diagnosis like single ANN model [21] and radial basis function (RBF) ANN model [22]. To avoid activate function in single ANN being too sensitive to diagnose PV fault effectively, different ANN models for different operation situations are developed [23]. In addition, Bayesian Neural Network (BNN) is developed and it is successfully implemented to diagnose soiling problems in PV arrays [24]. Moreover, fuzzy logic is reported that can improve model generalization performance when it is

applied on FDD [25] and it can perform well even if input features are limited [26]. The SSAMs based on a few labeled data for PV diagnosis are graph-based method [27] and clustering algorithm based PV fault diagnosis methods like density peak-based clustering [28], C-means clustering [29] and Gaussian kernel fuzzy C-means clustering [30], these methods can diagnose PV fault with only a few labeled PV data. These SSAMs can detect and diagnose many PV faults very effectively. However, The SSAMs do not perform well on detecting line-line fault (LLF) under low irradiance, which are challenging detecting cases [31].

Comparing with the above-mentioned SSAMs, TTDAMs focus on the new MPP searching procedure after faults occur. TTDAMs is a kind of signal analysis technology to analyze the transient in time domain through sequential PV data and quickly detects PVA faults [32], especially LLF [31]. For the last few years, several TTDAMs have been proposed and shown their capacity for FDD. Chen et al. introduce a quick detection algorithm for FDD based on the sequential change detection framework which only uses a minimal amount of meters [32]. This algorithm eliminates the delay of fault detection while it still needs further techniques to distinguish LLF from irradiance fluctuations. Yi et al. proposed an effectively fault detection method based on multi-resolution signal decomposition [9]. However, the accuracy of LLF under low line-line mismatch percentage still needs to be improved. After that, they use wavelet transform (WT) to extract feature from sequential PV data and a two stage SVM for classification so that better detection accuracy for different LLF can be obtained [31]. Although these two approaches acquire ideal detecting accuracy in simulation, their methods are not so effective for measured data, and these methods only detect LLF without classifying them. Similarly, the WT is used for feature extracting and then software for PVA fault diagnose is developed [33]. Moreover, an adaptive fast fault localization algorithm based on the measured power, voltage and irradiation is proposed in [34]. The way they used for PVA fault diagnose can detect LLF, ground fault and shading, while it needs each string PV data and more sensors should be implemented.

However, these TTDAMs may suffer from the following limitations: firstly, they require high-quality fault features [9,31,33]. These high-quality fault features demand experts to design fault features elaborately, which is highly time-consuming. Secondly, although detailed PV electrical data leads to a better diagnosing effect [34], it requires more sensors to obtain detailed PVA data. Therefore, these shortcomings of TTDAMs motivate us to search an approach that can extract feature from sequential PV data automatically without too much input. Recently, as a prosperous branch of Deep Learning (DL), Convolutional Neural Networks (CNNs) have been proven their powerful feature

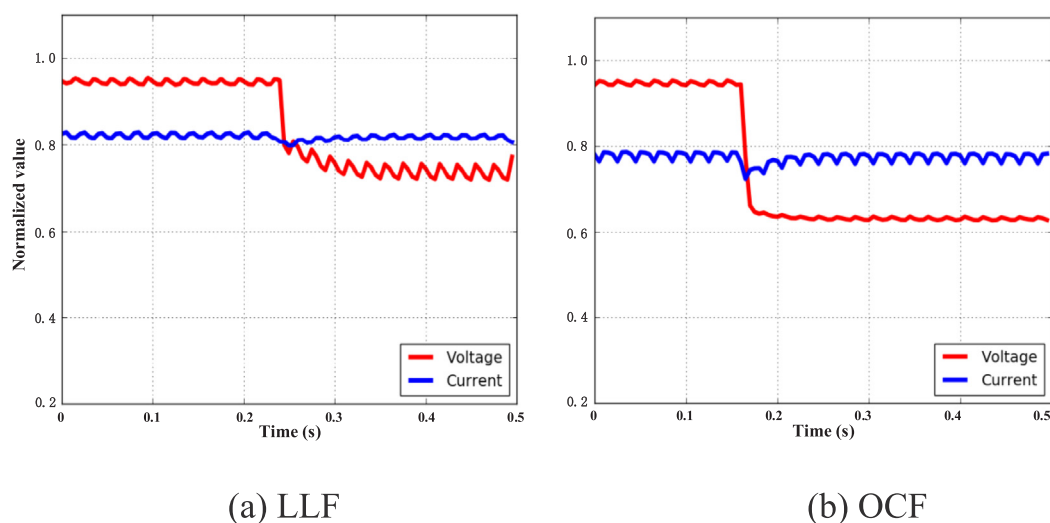


Fig. 6. PVA current and PVA voltage curve when faults happen.

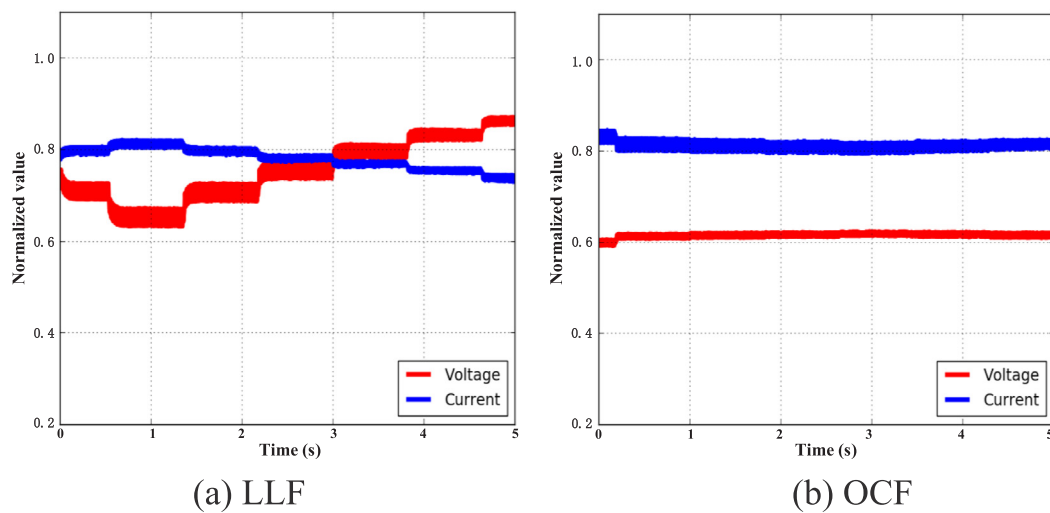


Fig. 7. The MPPT procedure after faults.

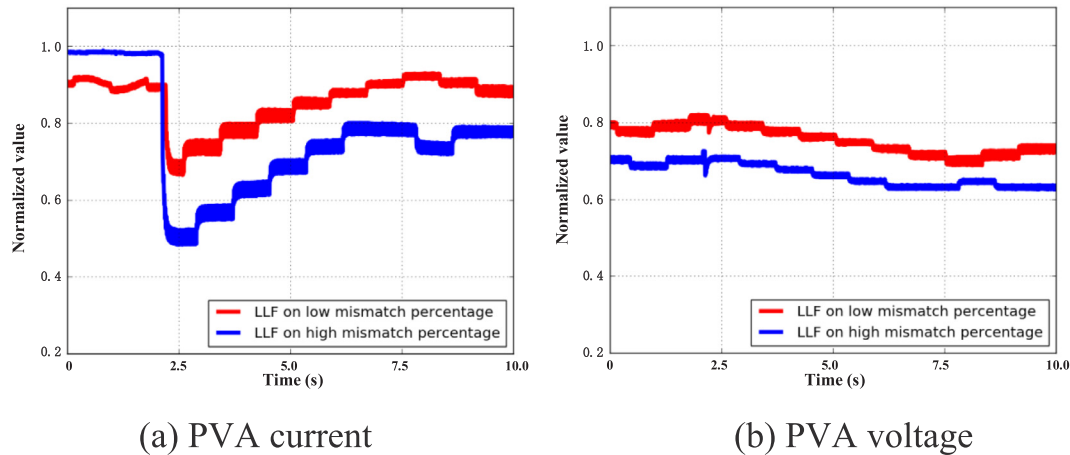


Fig. 8. LLF with different levels.

extracting ability [35]. CNNs are successfully applied to a larger variety of computer vision tasks and signal processing tasks, including object-detection [36], video classification [37], object tracking [38], super-resolution [39], and especially sequential electrocardiogram (ECG) identification [40]. In the literatures, ECG signals are processed by CNN to extract features and classify these features to diagnose coronary artery disease [41], arrhythmias [42] and myocardial infarction [43], which achieve impressive performance. Therefore, the success of CNN application in ECG inspires us to process sequential PVA data with CNN and then for FDD. Since there is a similarity between ECG with the sequential PVA data, both of them are a kind of signals with different variety tendency under different system conditions. Accordingly, in the article, the sequential PVA voltage and PVA current are transformed into electrical time series graph (ETSG), and then propose a model based on 2-Dimension (2D) CNN to automatically extract features from the input ETSG and subsequently diagnose faults.

The main achievements, including contributions of this work can be summarized as follows:

- 1) The 1-Dimension (1D) sequential PV data of transient in time domain is transformed into a 2D ETSG for FDD.
- 2) Only the sequential PVA voltage and sequential PVA current are used as the fault feature variables for the CNN based fault diagnosis model, and reference panels are used for data normalization.
- 3) A CNN structure consists of two-dimensional convolutional operations is proposed for the PVA fault diagnosis, which can extract fault

features from the sequential PVA voltage and PVA current automatically.

- 4) In contrast to the sequential fault diagnosis method (wavelet-SVM method) and Inception-V3 model of Google, the experiment results demonstrate that the proposed method has high accuracy and reliability.

The rest of the work are organized as follows: Section 2 introduces the PVS and the characteristics of transient in time domain of PVA. Section 3 elaborates the details of ETSG and the proposed CNN structure. Comprehensive fault experiments on a practical grid-connected PVS and corresponding results analysis are carried out in Section 4. Finally, the conclusions are reported in Section 5.

## 2. Photovoltaic system and the characteristics of transient in time domain of photovoltaic array

This section introduces a widely used typical PVS, illustrates the potential PV fault in PVS, and discusses the characteristics of transient in time domain of PV array.

### 2.1. Typical photovoltaic system

A typical grid-connected PVS consists of a PVA, an inverter with MPPT [44] and protection devices, such as overcurrent protection devices (OCPDs) and ground-fault protection devices (GFPDs) [45] as

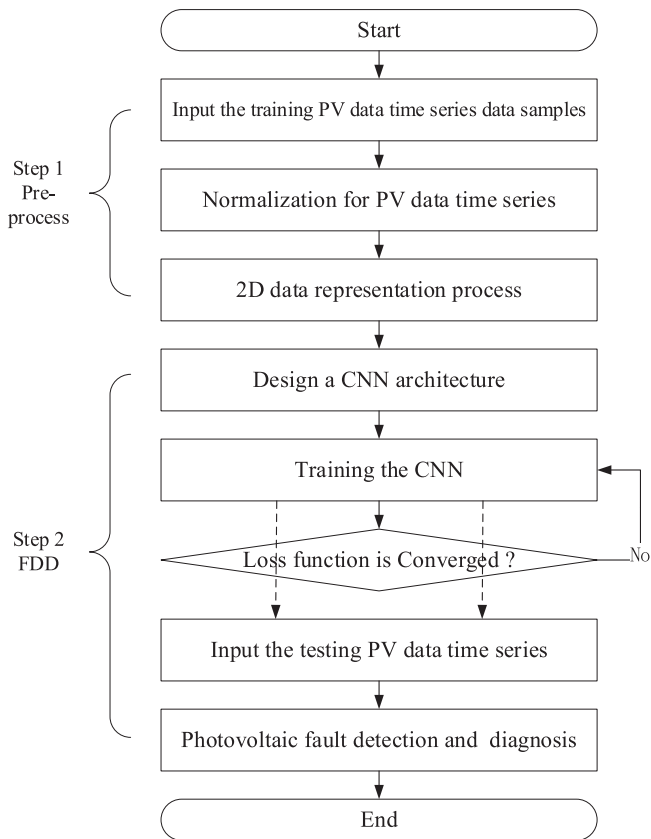


**Fig. 9.** Schematic diagram of the propose method.

shown in Fig. 1. In a PVA, PV panels connect in a series-and-parallel structure to outcome current and voltage. The characteristic curves and the operating point of a PVA change with the irradiance or temperature. To force the PVA work around the MPP, MPPT technology is applied in PVS to obtain the maximum power from the PVA. Typically, the MPPT is implemented by the DC/DC converter through maintaining the PV

output voltage at MPP. The inverter adjusts its DC-link voltage to track the reference  $V_{dc,r}$ , ensuring the output AC voltage of the inverter to match the grid voltage.

## 2.2. Faults in photovoltaic arrays

PVAs are prone to be encountered various faults, and a detailed analysis on various fault possibilities in PVAs is presented in [46]. PVA faults mainly include bypass diode failures, open-circuit fault (OCF), arc fault, ground fault, and LLF. This paper focuses on LLF and OCF, which are considered in Fig. 1. A LLF is an unintentional short circuiting connection between two points in the array with different potentials. The LLF may take place between two points in the same string or among two adjacent strings. It may be undetected and leads accidents [47]. The OCF is a kind of mismatch faults might occur because of cracked solar cells, blown fuse, or solder joint failure [48].

## 2.3. The characteristics of transient in time domain

This section focuses on the characteristics of transient in time domain, and these characteristics of transient in time domain are analyzed through sequential PV data collected from simulated PVS, including simulated 4 (parallel)  $\times$  7 (series), 7 (parallel)  $\times$  8 (series), and 8 (parallel)  $\times$  8 (series) grid connected PVS. As shown in Figs. 2–4, there are different tendencies can be observed when different PV faults (LLF and OCF) happen, which are fault characteristics of transient in time domain. It can be seen from Figs. 2–4, different PV fault can result in different tendencies in the same simulated PVS and the same type of PV fault has similar characteristics of transient in time domain in different PVS. Based on above simulation results, it can be concluded that LLF or OCF has their own characteristics of transient in time domain and these features can be used to diagnose PV fault in a PVS.

To verify the inferences derived from the simulation systems, a practical 3 (parallel)  $\times$  6 (series) grid connected PVS is built. Fig. 5 illustrates the normalized operating curves consist of sequential PVA current and sequential PVA voltage under normal conditions (NORMAL) in this practical PVS. As shown in the Fig. 5, the operating curves change smoothly in a certain period of time. However, the curves change drastically when a fault happens, as is shown in Fig. 6. In

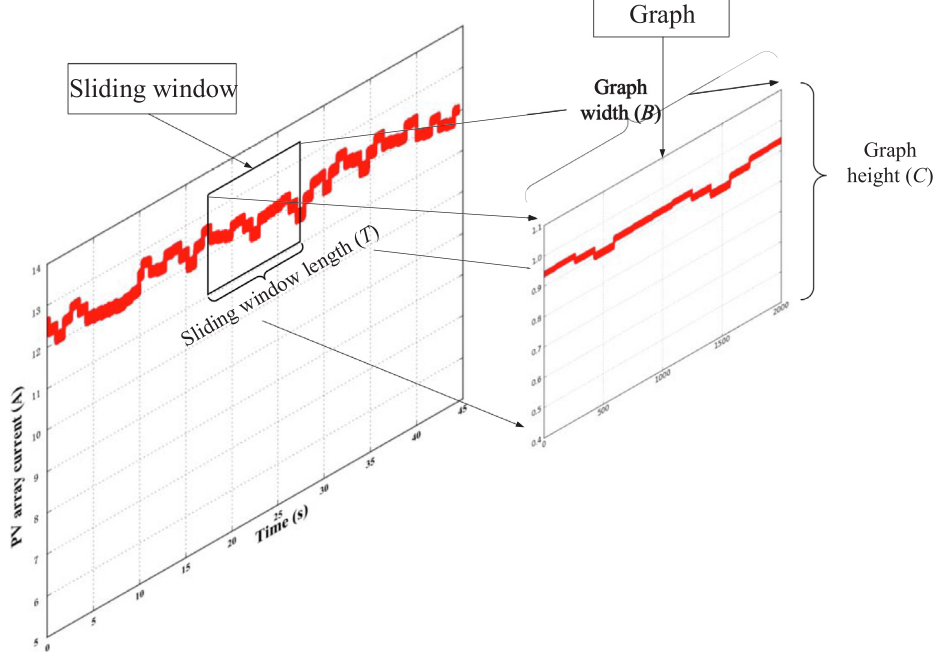
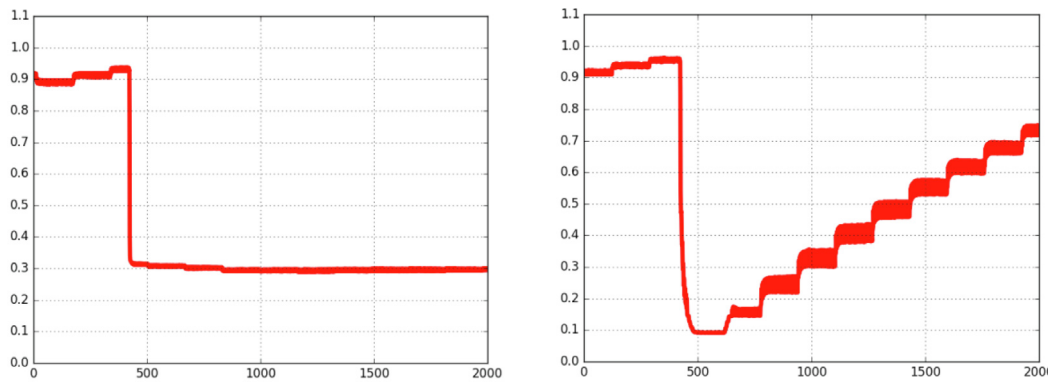


**Fig. 10.** The acquisition of 2D graph by using sliding window.



(a) Current graph of OCF

(b) Current graph of LLF

Fig. 11. The 2D graph.

addition, the severely reduced of PVA current can result in a significant drop in the output power of the PVA. In order to maintain the maximum power output after faults occur, the PVA current and PVA voltage are adjusted by MPPT to search a new MPP. As is depicted in Fig. 7, under different fault conditions, MPPT leads different changes in PVA current and PVA voltage. The PVA current and PVA voltage constantly change to search a new MPP when a LLF happens. Comparatively, after an open-circuit happens, MPPT do not result a substantially adjust of the PVA current and voltage.

As can be observed from Figs. 5–7, the curves of PVA voltage and PVA current under NORMAL condition and fault procedure are different obviously. Hence, the faults can be effectively detected through analyzing the change tendency of the sequential PV data [9,31]. Furthermore, the further comparison of the tendency between these faults can be applied to classify the type of faults, such as classification for the LLF and the OCF. However, there is similar tendency in a same category of fault under different levels, as shown in Fig. 8, which remains difficulty for detail fault classification. As illustrated in Fig. 8, a LLF with a low mismatch percentage and a LLF with a high mismatch percentage in a PVS are similar in variation tendency. By comparing the whole transient procedure of the two LLF, the current of the LLF with high mismatch percentage changes more drastically. Moreover, these curves are described by sequential PV data that consists of a series of points. Among these sequential points, there are some points reserve main information about the curve, namely key points (KPs), and the rest points may be less useful. For this reason, it can be concluded that the FDD can be implemented through analyzing KPs. Therefore, a CNN structure is designed to extract features, i.e. a series of KPs, from sequential PV data automatically and then apply these exacted KPs to FDD.

### 3. Methods

The proposed method contains two steps: the pre-process step and then followed the CNN based PVA fault diagnosis step. Fig. 9 sketches the flowchart of the proposed approach. Practically, the pre-process includes input normalization and 2D data representation. After pre-process, a designed CNN structure is implemented for FDD. In order to evaluate the performance of the model, the labeled samples are divided into two parts (the training dataset and the testing dataset). The training dataset is used to train CNN model until it is converged, while the testing dataset is used to test the model performance.

#### 3.1. Pre-process

Before 2D data representation process, the sequential PV data

should be normalized. Open-circuit voltage and short-circuit current of reference PV panels are used for normalizing the sequential PV data. Reference PV panels and PV system are placed in the same working environment, which the open-circuit voltage and short-circuit current of reference PV panels can reflect the environment temperature and solar radiation indirectly [27,49]. The sequential PV data is normalized by following formulas:

$$I_{\text{NORM}} = \frac{I_{\text{PVA}}}{P \cdot I_{\text{REF-SC}}} \quad (1)$$

$$V_{\text{NORM}} = \frac{V_{\text{PVA}}}{S \cdot V_{\text{REF-OC}}} \quad (2)$$

where,  $P$  means the number of parallel PV strings in the array and  $S$  is the number of PV modules in series in each PV string;  $I_{\text{REF-SC}}$ ,  $V_{\text{REF-OC}}$  are current and voltage of reference PV panels respectively. Hereafter,  $I_{\text{NORM}}$  and  $V_{\text{NORM}}$  are the normalized data.

To extract features from the raw sequential PV data by the CNN, as shown in Fig. 10, part of the sequential PV data by a  $T$  length sliding window is intercept and the intercepted sequential PV data is transform into a  $B \times C$  graph whose X-axis represents the PV data point and Y-axis represents the normalized value. Then, the sliding window slides over the whole sequential PV data to generate a series of 2D graphs and finally each graph is input into the CNN model for FDD. In the graph, the original normalized sequential PVA current data is transformed into a curve in graph, as depicted in Fig. 11.

The 2D graph visually reflects the feature of the PVA current data under different fault conditions. Furthermore, sequential PVA voltage is also a basic indicator of PVS which reflects the voltage tendency of a PVS. Both PVA current and PVA voltage are electrical characteristics of PVS. To effectively utilize different electrical characteristics of PVS, PVA current and PVA voltage are drawn in a graph that is named electrical time series graph (ETSG). To reduce useless information in ETSG, the grid with horizontal and vertical line in graphs and the number of normalized current and voltage in Y axis are removed, as Fig. 12 shows that the ETSG of different faults in the aforementioned PVS, including open circuit on two strings (OC-2), open circuit on one string (OC-1), short-circuit with 16.67% mismatch percentage (LL-1), short-circuit with 33.33% mismatch percentage (LL-2) and NORMAL. With the 2D representation operation, the sequential PV data is expected to reserve the useful information, which is learned by the following CNN.

#### 3.2. Convolutional neural networks

The CNN architecture is made up of two components. The first

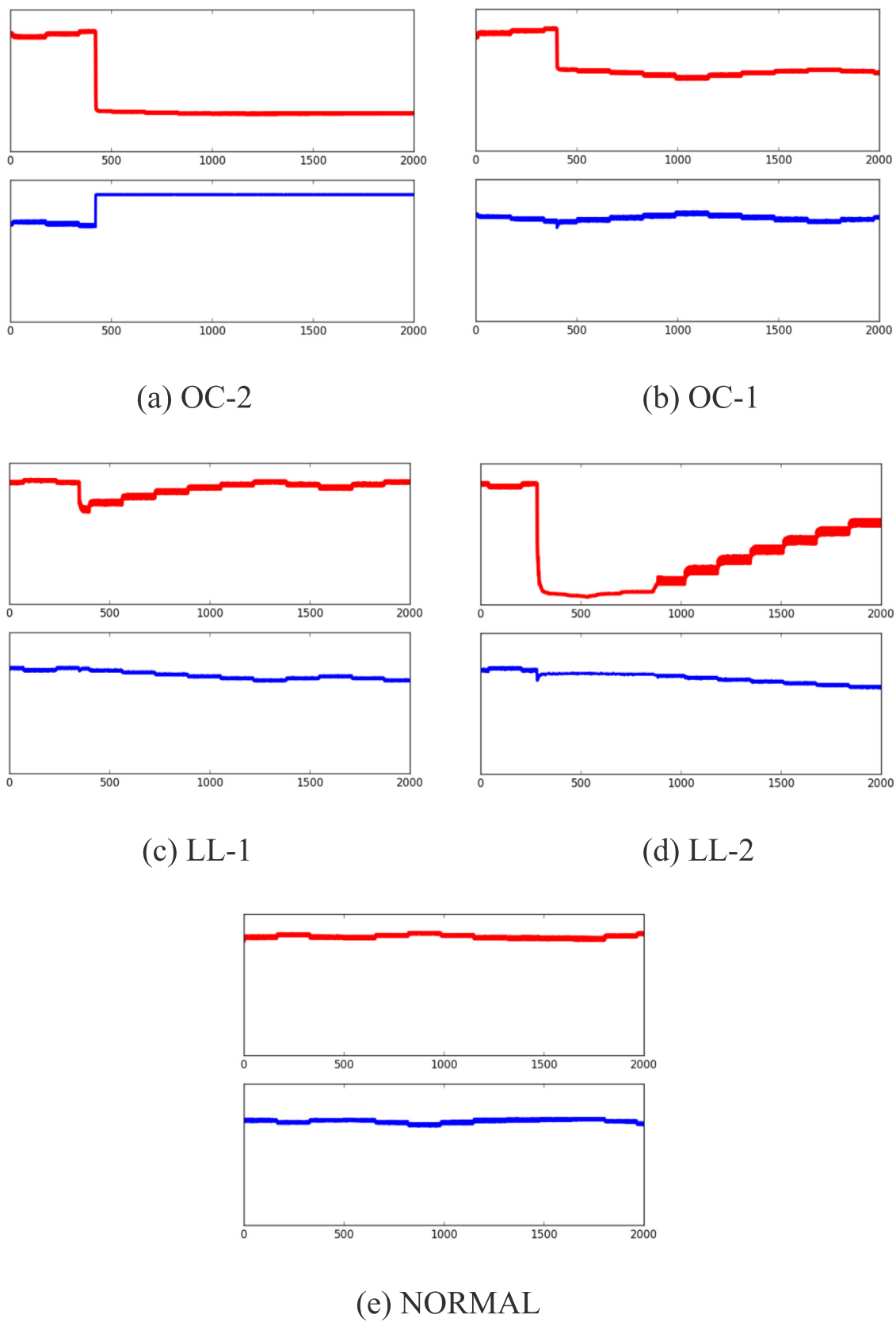


Fig. 12. ETSG.

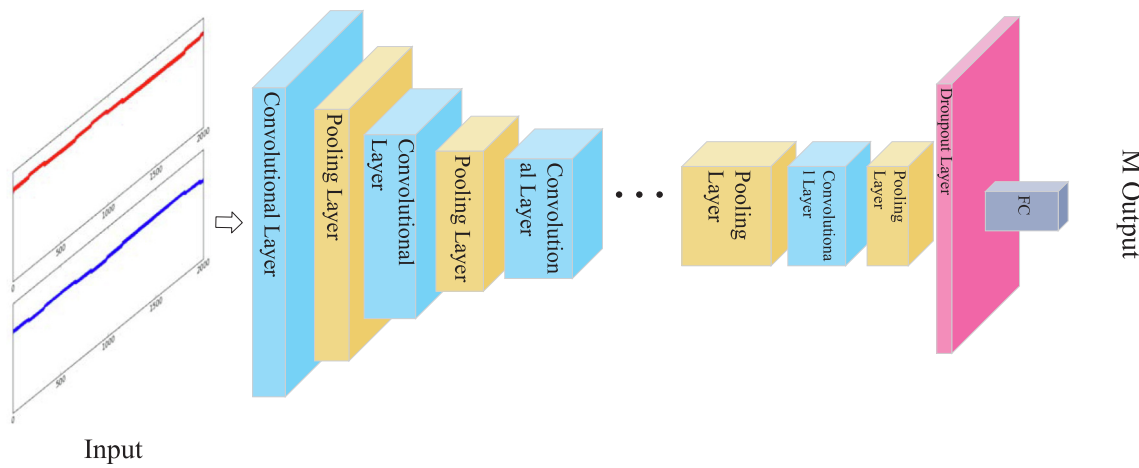


Fig. 13. The proposed CNN structure.

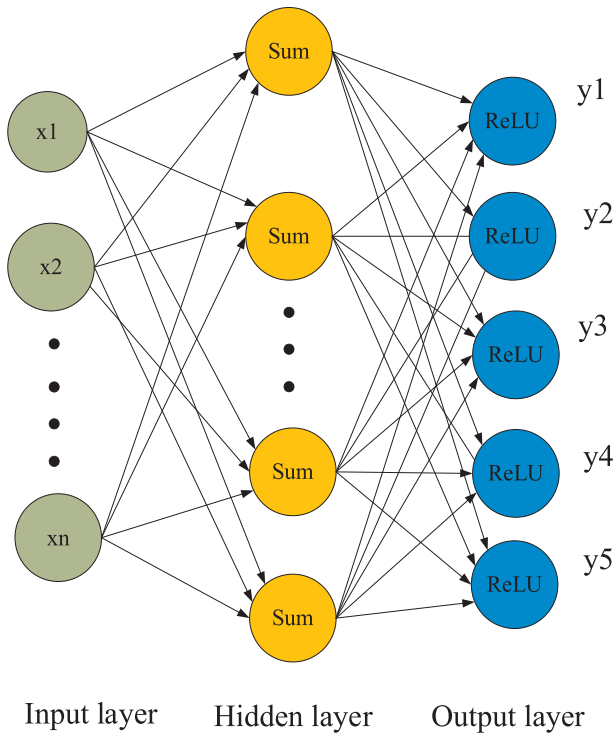


Fig. 14. Fully connected layer.

component is the feature extractor where features from the input data are learned automatically. The second component is a fully connected layer which carries out classification based on the initially learned features [50]. The structure of the proposed CNN model for PVA fault diagnosis is illustrated in Fig. 13. This CNN structure is made up of a series of alternating convolutional layers, max pooling layers, followed by a dropout layer and a fully connect layer (FC).

### 3.2.1. Convolutional layer

In convolutional layer, convolutional operation is applied to the input to extract the features. Neurons in different layers are locally connected via weight sharing technique. Convolutional layers contain lot of parameters which are named kernels. Every kernel has its receptive fields and corresponds to a full depth of the input. In the feed-forward process, a convolution operation is completed by a kernel, which calculates a dot product between the kernel and input in order to generate 2D representation of the kernel which is named feature map. After an activation function operation, the feature map is generated by the representation, which is computed as follows:

$$y_j^l = f(\sum_{i \in M_j} x_i^{l-1} \otimes w_{ij}^{l-1} + b_j^l) \quad (3)$$

where  $\otimes$  indicates the convolutional operation.

### 3.2.2. Pooling layer

By learning graph features using filters, convolutional layer preserves the spatial relationship between input and output. After convolutions, new feature map corresponds to enormous features extracted from input, which impedes the efficiency of calculation. An efficient

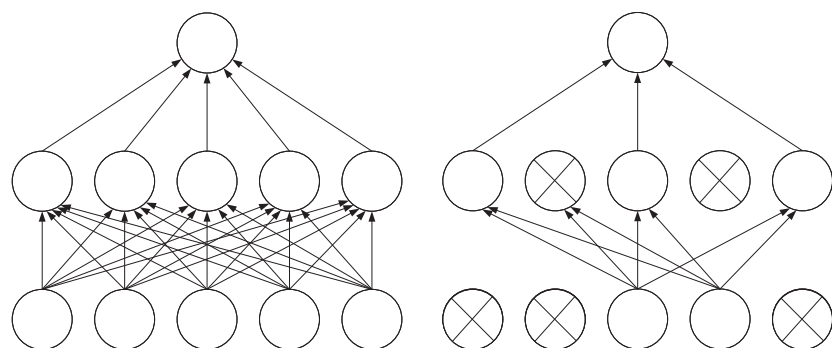


Fig. 15. Dropout Neural Net Model.

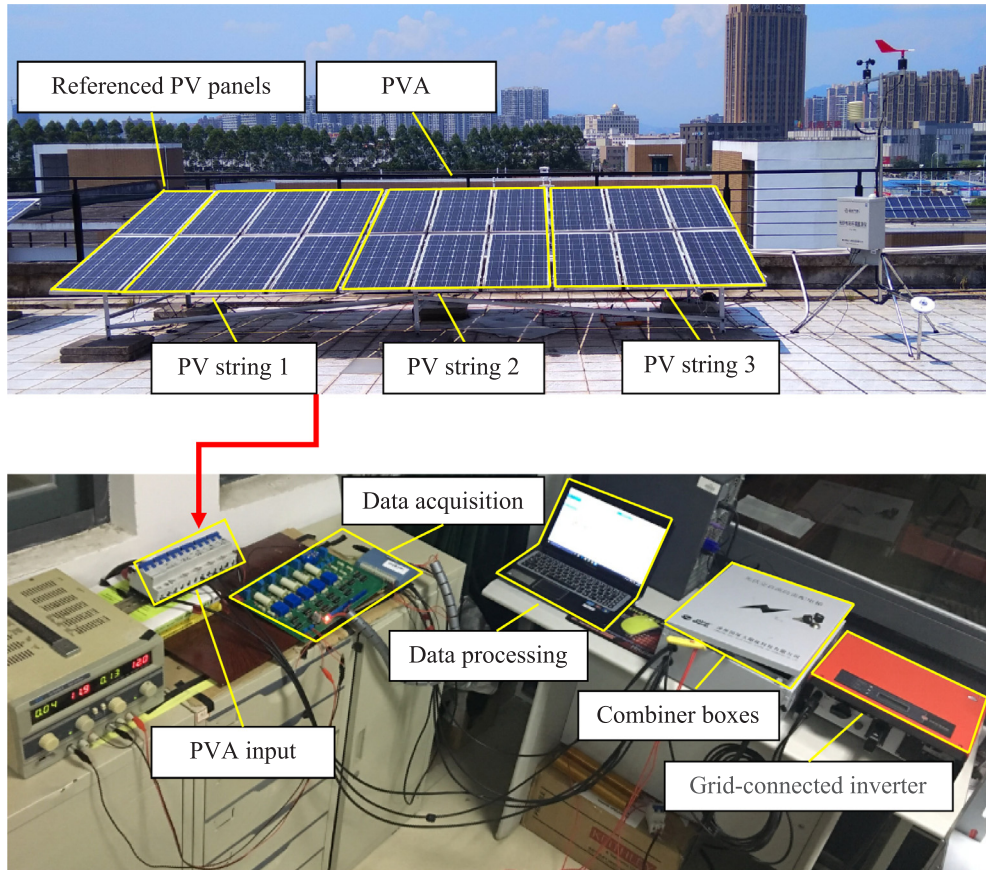


Fig. 16. The experimental platform.

**Table 1**  
Parameters of the Experimental Photovoltaic Array.

Devices	Module	Parameters
PVA	GL-100	STC: $P_{MPP} = 1800 \text{ W}$ , $V_{MPP} = 105 \text{ V}$ , $I_{MPP} = 17.1 \text{ A}$ , $V_{OC} = 129 \text{ V}$ , $I_{SC} = 18.1 \text{ A}$

solution to this problem is applying pooling layer to reduce redundant features. The input feature map is firstly divided a set of subareas, then they are converted to a more concise representation through a down-sampling operation, which is computed as follows:

$$y_j^l = f(\sum_{i \in M_j} \text{down}(x_j^{l-1}) \cdot \alpha_j^l + c_j^l) \quad (4)$$

where the down-sampling function ( $\text{down}(\cdot)$ ) can be an average pooling or a max pooling [51]. And the vector  $x$  in (4) contains the input values from a local pooling region of  $N$  pixels (typical pooling region dimensions are  $2 \times 2$  or  $3 \times 3$ ) in a channel or an image. In the article, the max pooling layer is chosen as the pooling layer in the proposed CNN structure that only outputs the max value of input region.

### 3.2.3. Fully connected layer

Convolutional component extracts feature from input, these features are input into a fully connected layer for classification. A fully

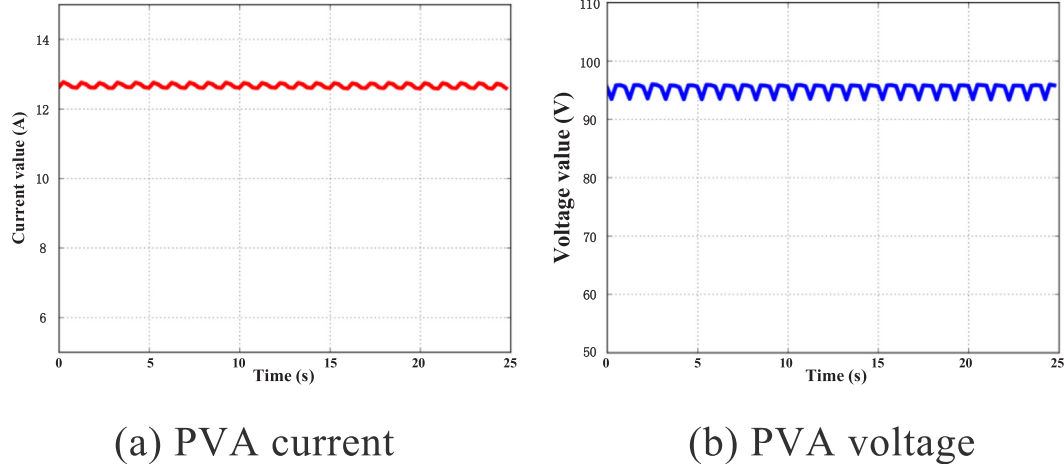
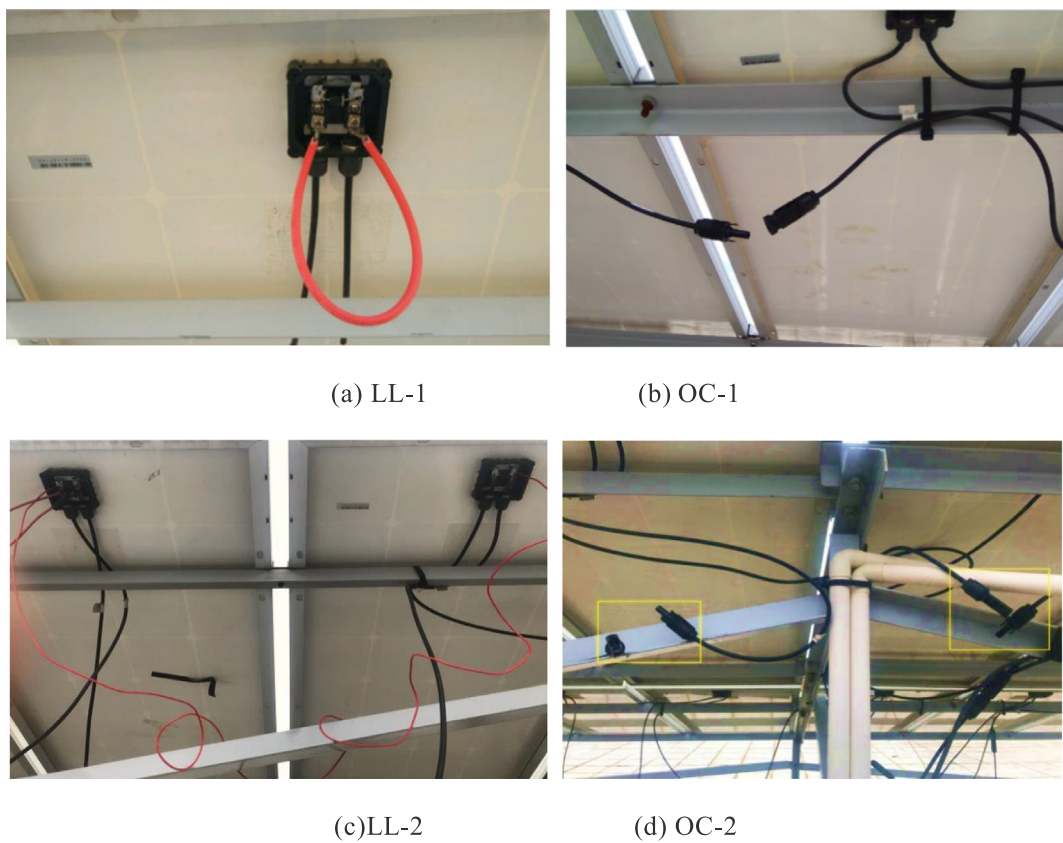


Fig. 17. Current and voltage under NORMAL.



**Fig. 18.** Experiment for faults: (a) LL-1; (b) OC-1; (c) LL-2; (d) OC-2.

**Table 2**  
Parameters of serve.

Device	Parameter
CPU	Intel i7 6700 K
GPU	NVIDIA GTX 1070
RAM	16 GB
RAM of GPU	8 GB

**Table 3**  
The dataset for CNN model.

Items	Normal	OC1	OC2	LL1	LL2
Total samples	422	300	178	322	178
Training samples	295	210	125	226	125
Testing samples	127	90	53	96	53

**Table 4**  
The detailed overview of proposed CNN structure.

Layers	Type	No. of kernels	Kernel size	Stride
1,2	Con/Max-pooling	16	5 × 5	1/2
3,4	Con/Max-pooling	32	5 × 5	1/2
5,6	Con/Max-pooling	64	3 × 3	1/2
7,8	Con/Max-pooling	128	3 × 3	2/2
9,10	Con/Max-pooling	256	3 × 3	2/2
11,12	Con/Max-pooling	512	1 × 1	2/2
13,14	Con/Max-pooling	1024	2 × 2	2/2
15,16	Con/Max-pooling	256	1 × 1	2/2
17,18	Con/Max-pooling	128	1 × 1	2/2
19	Dropout	–	–	–
20	Fully connected	–	–	–

connected layer is a neural network (NN) which is built from interconnected neurons. The theory of NN is described in the literature [52], and it is introduced briefly in the article, a neuron takes  $n$  input values  $x_1, \dots, x_n$ , and transforms them into one output value  $y$ .

$$y = f\left(\sum_{i=1}^{i=n} k_i x_i - bias\right) \quad (5)$$

where  $k_i$  refers to the sensitivity of a neuron to input values, and the *bias* that controls the overall importance of the input. The activation function means the reaction level of a neuron to input.

As illustrated in Fig. 14, neurons are organized in layers in the fully connect layer: an input layer with nodes  $x_n$ , an output layer with nodes  $y_i$ , and a hidden layer in between. The flatten features is an  $n$  dimension vector and they, in the article, will be transformed into a 5-Dimension output after fully connect layer processing, where each element stands for the probability of different states (NORMAL, LL-1, LL-2, OC-1, OC-2).

### 3.2.4. Dropout layer

Deep CNN structure is a very powerful system with large number parameters. However, over-fitting is a tricky problem in CNNs. To deal with the problem, Dropout technique is applied in CNNs to address this problem. Dropout operation randomly drops connection of units in training stage. This prevents units from co-adapting too much. As is shown in Fig. 15, some units selected in training period are inactive, and then only parts of units are trained. At test time, all units are active, and then a complete model can have a good performance without overfitting [53].

### 3.3. Optimization method

In order to obtain higher classification accuracy, it is necessary to

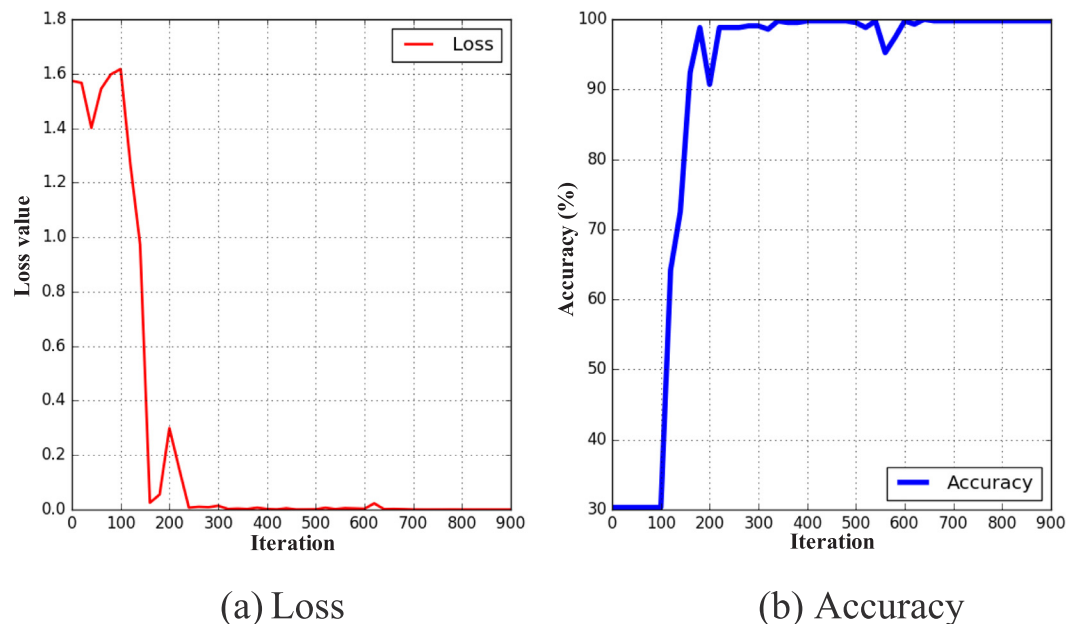


**Fig. 19.** Model loss and accuracy.

**Table 5**  
Confusion matrix of  $32 \times 32$  graph size.

Original/Predict	Normal	Open1	Open2	Short1	Short2	Sen (%)	Spec (%)	Speed (fps/s)
Normal	2531	0	0	3	6	99.65	99.83	0.0092
Open1	0	1799	1	0	0	99.94	99.98	0.0092
Open2	0	0	1060	0	0	100	99.92	0.0092
Short1	1	0	1	1904	14	99.17	99.80	0.0092
Short2	9	1	4	10	1036	97.74	99.72	0.0092

**Table 6**  
Confusion matrix of  $64 \times 64$  graph size.

Original/Predict	Normal	Open1	Open2	Short1	Short2	Sen (%)	Spec (%)	Speed (fps/s)
Normal	2534	3	0	3	0	99.76	99.74	0.010
Open1	5	1795	0	0	0	99.72	99.92	0.010
Open2	0	0	1060	0	0	100	99.93	0.010
Short1	2	0	0	1905	13	99.22	99.83	0.010
Short2	8	2	5	8	1037	97.83	99.82	0.010

**Table 7**  
Confusion matrix of  $299 \times 299$  graph size.

Original/Predict	Normal	Open1	Open2	Short1	Short2	Sen (%)	Spec (%)	Speed (fps/s)
Normal	2533	0	0	5	2	99.72	99.85	0.011
Open1	2	1798	0	0	0	99.89	100	0.011
Open2	0	0	1060	0	0	100	99.92	0.011
Short1	1	0	0	1905	14	99.22	99.84	0.011
Short2	6	0	6	5	1043	98.40	99.78	0.011

**Table 8**  
Accuracy of different input graph sizes.

Item	32 × 32 size	64 × 64 size	299 × 299 size
Accuracy (%)	99.40	99.42	<b>99.51</b>

optimize network parameters with optimization algorithm [54]. In the article, Adam algorithm is chosen as the optimization method which is an efficient stochastic optimization method to optimize CNN model [55]. Adam calculates sensitivity of neurons through back propagation

algorithm (BP) [56], so that model parameters can be updated to acquire better performance. Loss function is utilized to measure the quality of model, and loss function generates a unitless number, i.e., loss value, to describe the closeness between the model output and the target result. In our work, the loss function optimized by Adam is cross-entropy between real target labels and prediction labels as follows:

$$Loss = - \sum_{i=1}^N y_i \log P_i \quad (6)$$

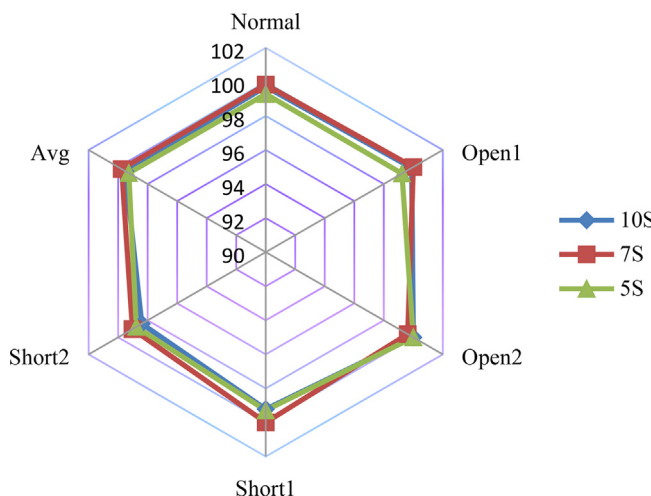


Fig. 20. Results of the proposed model under three sliding windows.

Table 9

Average accuracy of different input size of three sliding windows.

items	5 s sliding window	7 s sliding window	10 s sliding window
32 × 32 size	99.03%	99.30%	<b>99.40%</b>
64 × 64 size	99.16%	99.32%	<b>99.42%</b>
299 × 299 size	99.28%	99.40%	<b>99.51%</b>

$$P_i = \frac{e^{a_i}}{\sum_{k=1}^K e^{a_k}} \quad (7)$$

where  $P_i$  is the output of soft-max function for multi-classification problem and  $y_j$  is a label;  $K$  means the number of fault types and  $N$  is the number of training batch.

Adam algorithm has hyper-parameters learning-rate (LR) and two exponential decay rates ( $\beta_1$  and  $\beta_2$ ) should be determined, which have impacts on searching proper weights in CNN layers. The LR determines the upper limit of weight optimization in each iteration. The  $\beta_1$  and  $\beta_2$  determine the optimization degree for weights of CNN in each iteration. After these hyper-parameters are set, a CNN can be trained periodically. In each period, all parameters in CNN are updated once through Adam algorithm. The update operation is repeated until this model has converged, which means it is the end of the training process and the trained model can be used for FDD.

#### 4. Experimental results and discussion

In this section, the proposed CNN architecture for PVA fault diagnosis has been comprehensively assessed and benchmarked by using sequential PV data collected from a PVS in Fuzhou University.

##### 4.1. Experimental setup and procedures

The experimental platform is used to verify the proposed CNN model. The PVS illustrated in Fig. 16 consists of 3 (parallel) × 6 (series) PV panels which detailed parameters are depicted in Table 1 and the two PV modules on the left of the String 1 are reference panels. A convert is used to interface the PVA and deliver power to the grid. A data acquisition board collects sequential PVA current and sequential PVA voltage. Fig. 17 illustrates the real-time PVA current and PVA voltage of the experimental PVS under NORMAL. The experimental set up with the different faults configurations and the test facility are shown in Fig. 18a-d respectively. The types of the fault are the same as the aforementioned fault types of the PVS in Section 2, which includes LLF scenario with 1 module difference (LL-1), it has a 16.67% (1/6) location mismatch, LLF scenario with 2 module difference (LL-2), it has a 33.33% (2/6) location mismatch, OCF on 1 string (OC-1) and OCF on 2 strings (OC-2).

The ETSG is analyzed via a serve. In the serve, the CUDA platform from NVIDIA is used, and the CNN code is implemented using the Pytorch Library. Table 2 shows the detailed parameters of the serve. The total 1400 ETSG samples are collected under five conditions (NORMAL, OC-1, OC-2, LL-1, LL-2). Different input graph sizes  $B \times C$  (64 × 64, 128 × 128, 299 × 299) are selected to test the sensitivity of the model about the input size of ETSG. Furthermore, three different lengths of sliding window are designed, i.e.,  $T$  equals 10 s, 7 s, and 5 s respectively, to verify the stability of proposed CNN model.

##### 4.2. Experiment results

A total 1400 ETSG set of sequential PV data are collected from the experiment platform contains is randomly divided into two datasets, including training dataset with 981 (70%) samples, testing dataset with 419 (30%) samples, as shown in Table 3.

To extract the most suitable fault characteristics from ETSG, several convolution size kernels are applied to the proposed CNN model. Furthermore, a dropout layer is added to prevent over-fitting in training stage. Table 4 shows the details of the proposed CNN model.

The sliding window length  $T$  is set to 10 s firstly to test the model.

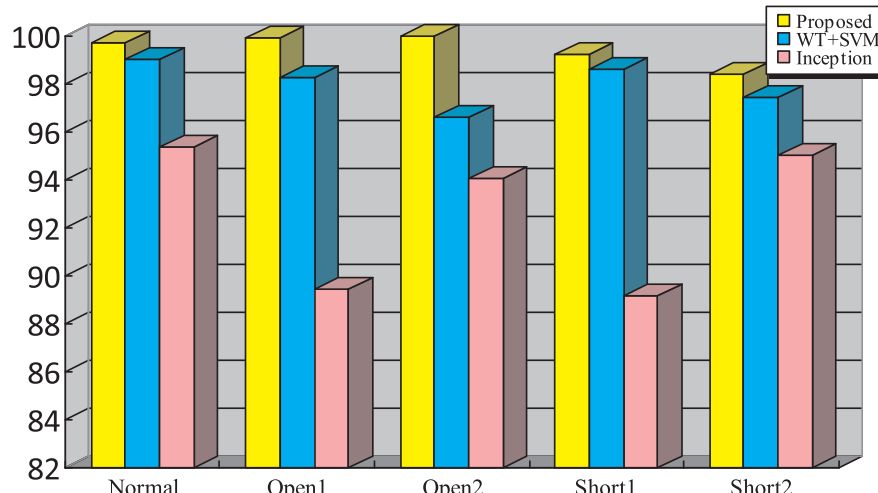
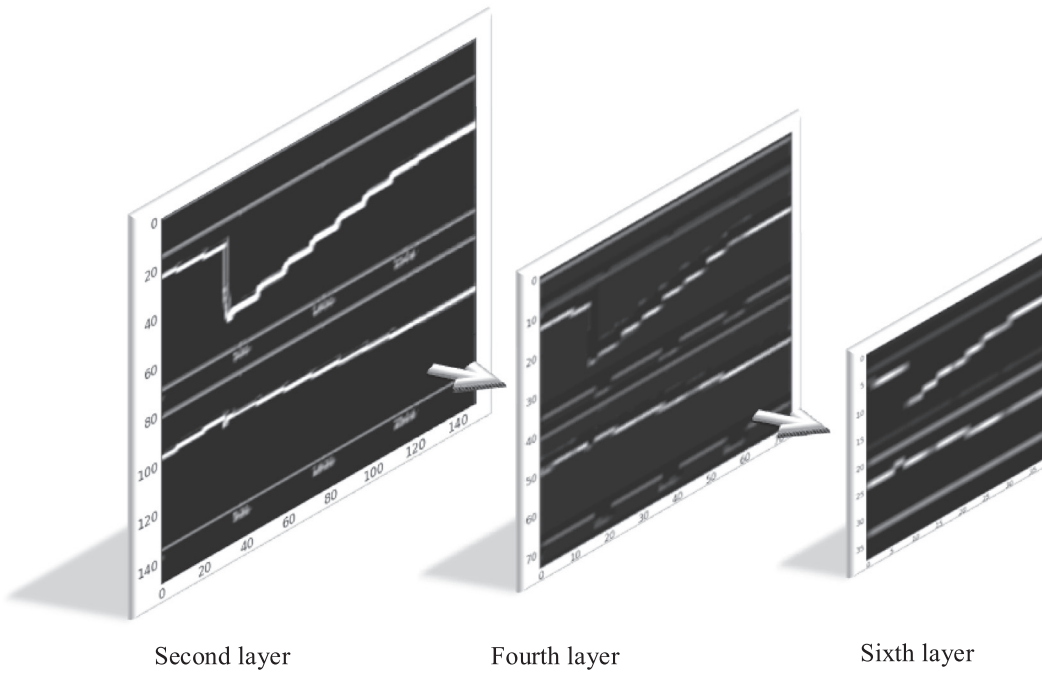


Fig. 21. Results of the three comparative methods.



**Fig. 22.** Feature map of different layers.

Before training the CNN, the hyper-parameters should be determined. Trial-and-error method is used to determine these hyper-parameters and it is found that the default hyper-parameters settings are ideal, which LR,  $\beta_1$ ,  $\beta_2$  are 0.001, 0.9 and 0.999 respectively [55]. The training process is shown in Fig. 19, where loss value of model is converged after the CNN model is optimized 900 iterations by Adam algorithm and the faults classification accuracy reaches the best value. The accuracy is the percent of correctly classified ETSG samples as follows:

$$\text{Accuracy} = \frac{\text{Correctly classified testing ETSG samples}}{\text{Total testing ETSG samples}} \quad (8)$$

The testing performance of the proposed CNN model refer to the selected three types of graphs size are summarized in three confusion matrix after 20 random tests, as shown in Tables 5–7 respectively. In these tables, *Sen* denotes the percentage of correctly identified positive data in actual positive data and *Spec* means the percentage of correctly identified negative data in actual negative data. Table 8 shows the corresponding average accuracy of the three types of input ETSG size. Therefore, it can be summed up from these tables that the proposed model with the three kinds of graph size can achieve high sensitivity and specificity, and the  $299 \times 299$  graph size obtains the highest accuracy.

In order to verify the stability of the proposed model, another two kinds of sliding windows, i.e.,  $T = 7\text{ s}$  and  $T = 5\text{ s}$ , are applied to the proposed model respectively. The accuracy under various fault conditions of different sliding windows is shown in Fig. 20. The results are summarized in Table 9. Different sliding windows do not result in significant changes in diagnostic accuracy, which exhibits the stability of proposed FDD approach.

To comprehensively test the overall performance of the proposed CNN model, Inception-V3 [57] and wavelet transform SVM (WT-SVM) methods are adopted for performance comparison. Inception-V3 is a deep CNN structure with strong feature extracted ability. WT and SVM have been applied on a lot of PV detection or diagnosis methods which achieved a good performance. In the experiment, ‘db10’ is chosen as wavelet basis for WT, the parameters,  $c$  and  $\gamma$  of SVM, are set to 1000 and 5 to obtain better performance. Ultimately, the comparison

result is shown in Fig. 21, and our method shows a better performance.

#### 4.3. Discussion

The proposed CNN structure for FDD is motivated by its powerful feature extracting and classifying ability that only requires PVA current and PVA voltage input. It is trained to be an automated feature extractor for sequential PV data. CNN is an end-to-end model which is consider as a black-box. Therefore, three layers output of the network are visualized to analyze the kinds of features are extracted from sequential PV data by the trained CNN. Fig. 22 illustrates the output feature maps in second layer, fourth layer and sixth layer of the trained CNN. It can be noted from Fig. 22 that the CNN model extracts curves and the coordinate axis in second layer, and then the extracted curves are analyzed in follow layers while coordinate axes are gradually ignored. In the followed layers, most of the redundant points in the curve are filtered out, and only some points are left, which feature map size reduces from  $149 \times 149$  to  $35 \times 35$  but it can still be roughly seen the complete curve. For this result, a possible explanation is that these convolutional layers extract KPs in these curves of ETSG to represent sequential PV data. Thus, the proposed CNN continuously extracts KPs in curves. Finally, the remaining data points represent a characteristic of the sequential PV data. In addition, there are many different convolution kernels in each CNN layer, and each convolution kernel extracts a kind of feature of the curve to create a feature map. Each feature map represents a set of KPs that represents a characteristic of sequential PV data. Afterwards, these features extracts by CNN are input to a fully connected layer to obtain the final classification output. Different fault inputs result in completely different extracting feature, so that fully connected layer can classify these faults easily. Comparing with different input graph size in Table 7, the improvement of accuracy is limited, but bigger input size better than smaller ones. Since smaller input size is processed with less pixel, once input size get smaller, some PV data points in input is missing. As a result, smaller input sizes cause information loss, although the loss have only a little influence on CNN model, it still leads a little drop on classification accuracy. Though the large input graph size is more time consuming as Table 5 shows, bigger input graph size ( $299 \times 299$ ) only needs 0.011 s to be processed, which

is acceptable in practically.

To explore the influence of different sliding windows on the proposed model, three kinds of sliding windows are tested in the experiment. Fig. 20 and Table 8 show clear evidence that different sliding windows also achieve good performance in testing. The proposed model using different sliding windows achieve over 99% average accuracy in testing dataset. Comparing to 10 s sliding window, the 5 s and 7 s sliding windows cannot cover the whole fault procedure, while our method can also have a good performance in testing data with these sliding windows, which shows the stability of the proposed model. Additionally, the length of sliding window roughly depends on the convergence rate of MPPT algorithm.

Furthermore, the performance of different PVA fault diagnosis method is evaluated under the same benchmark dataset, respectively. Fig. 21 summarizes the results of three different methods. Comparing to the Inception-V3 model and WT-SVM method, the proposed method has higher accuracy under different conditions. The input ETSG is not complex, but Inception-V3 model is a very deep CNN model, which extracts too much useless information and it causes a loss in accuracy, even learn nothing sometime. WT-SVM method extracts sequential PV data features by discrete wavelet transform (DWT), which may not optimal to reflect the underlying signal characteristics. Typically, our proposed method extracts enough useful information in sequential PV data, leading a better performance. Therefore, from above examples, it can be seen the PVA fault diagnosis model based on CNN and ETSG is appealing for practical implementations. Moreover, PVA faults in different PVS have similar variation characteristics during transient in time domain, it is possible that the trained model can be used to diagnose or detect faults for other PVA.

## 5. Conclusions

In this study, a fault diagnosis model for PVS based on CNN and ETSG is firstly proposed. Only normalized sequential PVA current and PVA voltage are transformed into an ETSG. This approach does not require elaborate designed fault features but fault features are automatically extracted from ETSG by CNN. The experiment is carried out to verify the performance of the proposed method. In the case study, the classification accuracies with different sliding windows on testing dataset are 99.28%, 99.40%, and 99.51% respectively. Furthermore, the comparison results show that the CNN and ETSG based approach exhibits better performance. Given our results, these suggest that the proposed CNN model achieve significant classification accuracy and stability for FDD. Therefore, the PVA fault diagnosis model based on CNN and ETSG has a high potential for practical applications in PVS. In the future, a further application of this model to other PVA will be conducted.

## Declaration of Competing Interest

The authors declare no conflict of interest.

## Acknowledgments

This work was supported by the National Natural Science Foundation of China (Grant Nos. 61574038, 61601127, and 51508105), the Foundation of Fujian Provincial Department of Science and Technology (Grant Nos. 2018J01774, 2018J01645 and 2019H0006), and the Fujian Provincial Economic and Information Technology Commission of China (Grant Nos. 82318075).

## References

- [1] Pillai DS, Rajasekar N. A comprehensive review on protection challenges and fault diagnosis in PV systems. *Renew Sustain Energy Rev* 2018;91:18–40.
- [2] Panwar NL, Kaushik SC, Kothari S. Role of renewable energy sources in environmental protection: a review. *Renew Sustain Energy Rev* 2011;15(3):1513–1524.
- [3] PVPS, I., Snapshot of global photovoltaic markets 2018. Report IEAPVPS; 2018.
- [4] Flicker J, Johnson J. Analysis of fuses for blind spot ground fault detection in photovoltaic power systems. Sandia National Laboratories Report 2013.
- [5] Karami Nabil, Moubayed Nazih, Outbib Rachid. General review and classification of different MPPT Techniques. *Renew Sustain Energy Rev* 2017;68:1–18.
- [6] Tey Kok Soon, et al. Improved differential evolution-based MPPT algorithm using SEPIC for PV systems under partial shading conditions and load variation. *IEEE Trans Ind Inf* 2018;14(10):4322–33.
- [7] Li Hong, et al. An overall distribution particle swarm optimization MPPT algorithm for photovoltaic system under partial shading. *IEEE Trans Ind Electron* 2019;66(1):265–75.
- [8] Zhao Y, et al. Line-Line Fault Analysis and Protection Challenges in Solar Photovoltaic Arrays. *IEEE Trans Ind Electron* 2013;60(9):3784–95.
- [9] Yi Z, Etemadi AH. Fault detection for photovoltaic systems based on multi-resolution signal decomposition and fuzzy inference systems. *IEEE Trans Smart Grid* 2017;8(3):1274–83.
- [10] Chen Z, et al. Intelligent fault diagnosis of photovoltaic arrays based on optimized kernel extreme learning machine and I-V characteristics. *Appl Energy* 2017;204:912–31.
- [11] Takashima T, et al. Experimental studies of fault location in PV module strings. *Sol Energy Mater Sol Cells* 2009;93(6–7):1079–82.
- [12] Roy S, et al. An irradiance independent, robust ground fault detection scheme for PV arrays based on spread spectrum time domain reflectometry (SSTD). *IEEE Trans Power Electron* 2018;33(8):7046–57.
- [13] Solórzano J, Egido MA. Automatic fault diagnosis in PV systems with distributed MPPT. *Energy Convers Manage* 2013;76:925–34.
- [14] Platon R, Martel J, Woodruff N, et al. Online fault detection in PV systems. *IEEE Trans Sustainable Energy* 2015;6(4):1200–7.
- [15] Tadj M, et al. Improving the performance of PV systems by faults GISTEL approach. *Energy Convers Manage* 2014;80:298–304.
- [16] Silvestre S, et al. New procedure for fault detection in grid connected PV systems based on the evaluation of current and voltage indicators. *Energy Convers Manage* 2014;86:241–9.
- [17] Mellit A, Kalogirou SA. Artificial intelligence techniques for photovoltaic applications: a review. *Prog Energy Combust Sci* 2008;34:574–632.
- [18] Zhao Y, et al. Decision tree-based fault detection and classification in solar photovoltaic arrays. In: 2012 Twenty-Seventh Annual IEEE Applied Power Electronics Conference and Exposition (APEC). IEEE, 2012.
- [19] Rezgui W, Mouss LH, Mouss NK, et al. A smart algorithm for the diagnosis of short-circuit faults in a photovoltaic generator. In: IEEE 2014 International Conference on Green Energy, 2014:139–143.
- [20] Chen Z, et al. Random forest based intelligent fault diagnosis for PV arrays using array voltage and string currents. *Energy Convers Manage* 2018;178:250–64.
- [21] Chine W, et al. A novel fault diagnosis technique for photovoltaic systems based on artificial neural networks. *Renewable Energy* 2016;90:501–12.
- [22] Dhimish M, et al. Comparing Mamdani Sugeno fuzzy logic and RBF ANN network for PV fault detection. *Renew Energy* 2018;117:257–74.
- [23] Karatepe E, Hiyama T. Controlling of artificial neural network for fault diagnosis of photovoltaic. 2011 16th International Conference on Intelligent System Applications to Power Systems. IEEE; 2011. p. 1–6.
- [24] Pavan AM, Mellit A, De Pieri D, Kalogirou SA. A comparison between BNN and regression polynomial methods for the evaluation of the effect of soiling in large-scale photovoltaic plants. *Appl Energy* 2013;108:392–401.
- [25] Dhimish M, et al. Photovoltaic fault detection algorithm based on theoretical curves modelling and fuzzy classification system. *Energy* 2017;140:276–90.
- [26] Belaout A, et al. Multiclass adaptive neuro-fuzzy classifier and feature selection techniques for photovoltaic array fault detection and classification. *Renew Energy* 2018;127:548–58.
- [27] Zhao Y, Ball R, Mosesian J, et al. Graph-based semi-supervised learning for fault detection and classification in solar photovoltaic arrays. *IEEE Trans Power Electron* 2015;30(5):2848–58.
- [28] Lin P, et al. A density peak-based clustering approach for fault diagnosis of photovoltaic arrays. *Int J Photoenergy* 2017;9:1–14.
- [29] Zhu Honglu, et al. Fault diagnosis approach for photovoltaic arrays based on unsupervised sample clustering and probabilistic neural network model. *Sol Energy* 2018;176:395–405.
- [30] Zhao Q, et al. A New PV Array Fault Diagnosis Method Using Fuzzy C-Mean Clustering and Fuzzy Membership Algorithm. *Energies* 2018;11(1):238.
- [31] Yi Z, Etemadi A. Line-to-line fault detection for photovoltaic arrays based on multiresolution signal decomposition and two-stage support vector machine. *IEEE Trans Ind Electron* 2017;64(11):8546–56.
- [32] Chen L, Li S, Wang X. Quickest fault detection in photovoltaic systems. *IEEE Trans Smart Grid* 2018;9(3):1835–47.
- [33] Kumar BP, et al. Online Fault Detection and Diagnosis in Photovoltaic Systems Using Wavelet Packets. *IEEE J Photovoltaics* 2018;8(1):257–65.
- [34] Chen L, Wang X. Adaptive fault localization in photovoltaic systems. *IEEE Trans Smart Grid* 2017;9(6):6752–63.
- [35] Alex Krizhevsky, Sutskever I, Hinton G. Imagenet classification with deep convolutional neural networks. *Neural Information Process Syst* 2012:1097–105.
- [36] Ren S, He K, Girshick R, Faster R-CNN, et al. Towards Real-Time Object Detection with Region Proposal Networks. *Neural Information Process Syst* 2015:91–9.
- [37] Karpathy A, Toderici G, Shetty S, et al. Large-scale video classification with convolutional neural networks. Proceedings of the IEEE conference on Computer Vision

- and Pattern Recognition. 2014. p. 1725–32.
- [38] Bertinetto L, Valmadre J, Henriques JF, et al. Fully-convolutional siamese networks for object tracking. European conference on computer vision. 2016. p. 850–65.
- [39] Lai WS, et al. Deep laplacian pyramid networks for fast and accurate super-resolution. IEEE Conference on Computer Vision and Pattern Recognition 2017;2(3):5835–43.
- [40] Kiranyaz S, Ince T, Gabbouj M. Real-time patient-specific ECG classification by 1-D convolutional neural networks. *IEEE Trans Biomed Eng* 2016;63(3):664–75.
- [41] Acharya UR, et al. Automated detection of coronary artery disease using different durations of ECG segments with convolutional neural network. *Knowl-Based Syst* 2017;132:62–71.
- [42] Acharya UR, et al. Automated detection of arrhythmias using different intervals of tachycardia ECG segments with convolutional neural network. *Inf Sci* 2017;405:81–90.
- [43] Acharya UR, et al. Application of deep convolutional neural network for automated detection of myocardial infarction using ECG signals. *Inf Sci* 2017;415:190–8.
- [44] Romero-Cadaval Enrique, et al. Grid-connected photovoltaic plants: An alternative energy source, replacing conventional sources. *IEEE Ind Electron Mag* 2015;9(1):18–32.
- [45] U.S. National Electrical Code. Article 690—Solar Photovoltaic Systems 2011.
- [46] Triki-Lahiani A, Abdelghani ABB, Slama-Belkhodja I. Fault detection and monitoring systems for photovoltaic installations: a review. *Renew Sustain Energy Rev* 2017;82:2680–92.
- [47] Sharma V, Chandel SS. Performance and degradation analysis for long term reliability of solar photovoltaic systems: a review. *Renew Sustain Energy Rev* 2013;27:753–67.
- [48] Zhao Y, et al. Outlier detection rules for fault detection in solar photovoltaic arrays. 2013 Twenty-Eighth Annual IEEE Applied Power Electronics Conference and Exposition. 2013. p. 2913–20.
- [49] Yahyaoui Imene, Segatto Marcelo EV. A practical technique for on-line monitoring of a photovoltaic plant connected to a single-phase grid. *Energy Convers Manag* 2017;132:198–206.
- [50] Zubair M, Kim J, Yoon C. An automated ECG beat classification system using convolutional neural networks. 6th International Conference on IT Convergence and Security (ICITCS). 2016. p. 1–5.
- [51] Boureau YL, Ponce J, LeCun Y. A theoretical analysis of feature pooling in visual recognition. Proceedings of the 27th international conference on machine learning (ICML-10). 2010. p. 111–8.
- [52] Haykin SS, et al. Neural networks and learning machines. NJ, Englewood Cliffs: Prentice-Hall; 2009.
- [53] Srivastava N, et al. Dropout: a simple way to prevent neural networks from overfitting. *J Mach Learn Res* 2014;15(1):1929–58.
- [54] Bottou Léon, Curtis Frank E, Nocedal Jorge. Optimization methods for large-scale machine learning. *SIAM Rev* 2018;60(2):223–311.
- [55] Kingma Diederik P, Jimmy Ba. Adam: A method for stochastic optimization. In: International Conference on Learning Representations (ICLR), 2015: 1–41.
- [56] Wang H, et al. Deterministic and probabilistic forecasting of photovoltaic power based on deep convolutional neural network. *Energy Convers Manage* 2017;153:409–22.
- [57] Szegedy Christian, et al. Rethinking the inception architecture for computer vision. Proceedings of the IEEE conference on computer vision and pattern recognition. 2016. p. 2818–26.